Multi-objective design optimization of bioresorbable braided stents

Computer Methods and Programs in Biomedicine 242 (2023) 107781

Contents lists available at ScienceDirect

Computer Methods and Programs in Biomedicine

journal homepage: www.elsevier.com/locate/cmpb

Multi-objective design optimization of bioresorbable braided stents

Dario Carbonaro [a,1], Agnese Lucchetti [b,1], Alberto L. Audenino [a], Thomas Gries [b], Ted J. Vaughan [c,2], Claudio Chiastra [a,2,*]

[a] PoliTo[BIO]Med Lab, Department of Mechanical and Aerospace Engineering, Politecnico di Torino, Turin, Italy
[b] Institut für Textiltechnik of RWTH Aachen University, Aachen, Germany
[c] Biomechanics Research Centre (BioMEC), School of Engineering, College of Science and Engineering, University of Galway, Ireland

ARTICLE INFO

Keywords:
Critical limb ischemia
Bioresorbable braided stent
Bioresorbable polymer
Design optimization
Finite element analysis

ABSTRACT

Background and objectives: Bioresorbable braided stents, typically made of bioresorbable polymers such as poly-l-lactide (PLLA), have great potential in the treatment of critical limb ischemia, particularly in cases of long-segment occlusions and lesions with high angulation. However, the successful adoption of these devices is limited by their low radial stiffness and reduced elastic modulus of bioresorbable polymers. This study proposes a computational optimization procedure to enhance the mechanical performance of bioresorbable braided stents and consequently improve the treatment of critical limb ischemia.

Methods: Finite element analyses were performed to replicate the radial crimping test and investigate the implantation procedure of PLLA braided stents. The stent geometry was characterized by four design parameters: number of wires, wire diameter, initial stent diameter, and braiding angle. Manufacturing constraints were considered to establish the design space. The mechanical performance of the stent was evaluated by defining the radial force, foreshortening, and peak maximum principal stress of the stent as objectives and constraint functions in the optimization problem. An approximate relationship between the objectives, constraint, and the design parameters was defined using design of experiment coupled with surrogate modelling. Surrogate models were then interrogated within the design space, and a multi-objective design optimization was conducted.

Results: The simulation of radial crimping was successfully validated against experimental data. The radial force was found to be primarily influenced by the number of wires, wire diameter, and braiding angle, with the wire diameter having the most significant impact. Foreshortening was predominantly affected by the braiding angle. The peak maximum principal stress exhibited contrasting behaviour compared to the radial force for all parameters, with the exception of the number of wires. Among the Pareto-optimal design candidates, feasible peak maximum principal stress values were observed, with the braiding angle identified as the differentiating factor among these candidates.

Conclusions: The exploration of the design space enabled both the understanding of the impact of design parameters on the mechanical performance of bioresorbable braided stents and the successful identification of optimal design candidates. The optimization framework contributes to the advancement of innovative bioresorbable braided stents for the effective treatment of critical limb ischemia.

1. Introduction

Bioresorbable stents, typically made of bioresorbable polymers such as poly-l-lactide (PLLA), polycarbonate and polydioxanone, or bioabsorbable metals such as magnesium, offer a promising alternative to permanent metallic stents [1]. They possess the advantage of providing temporary vessel support for the required duration before gradually degrading into byproducts [2]. This characteristic provides several long-term benefits, including the prevention of late inflammation, reduction of artifacts in clinical images, prevention of complications in

Abbreviations: CLI, critical limb ischemia; D, Diameter; FE, finite element; FS, Foreshortening; PLLA, poly-l-lactide; PMPS, Peak maximum principal stress; RF, Radial force.

* Corresponding author.
E-mail address: claudio.chiastra@polito.it (C. Chiastra).

[1] D. Carbonaro and A. Lucchetti contributed equally to this work and are co-first authors.
[2] T.J. Vaughan and C. Chiastra contributed equally to this work and are co-last authors.

https://doi.org/10.1016/j.cmpb.2023.107781
Received 20 June 2023; Received in revised form 18 August 2023; Accepted 25 August 2023
Available online 26 August 2023

secondary surgeries, and reduced need of long-term antiplatelet treatment [2–4]. Bioresorbable stents are classified into laser-cut stents, which are fabricated by laser cutting tubular materials, and braided stents, which are composed of interlaced monofilaments that can move independently [5]. Bioresorbable laser-cut stents have shown promising results in treating short-segment occlusions in critical limb ischemia (CLI) [1]. However, these devices have demonstrated limited efficiency for the treatment of CLI in cases of long-segment occlusions and lesions with high angulations [6]. Conversely, bioresorbable braided stents offer superior conformability to the vessels, making them potentially valuable in treating these challenging lesions [7]. Nevertheless, the design of bioresorbable braided stents for CLI poses several challenges.

Notably, stents must generate adequate radial force to provide sufficient support to the blood vessel, ensuring vessel patency and preventing re-occlusion [8]. Regarding this, the lower radial stiffness of braided stents compared to laser-cut stents [9] and the reduced elastic modulus of bioresorbable polymers in comparison to metals [1] make the design of bioresorbable braided stents for CLI applications challenging. Furthermore, bioresorbable braided stents should exhibit minimal foreshortening, referring to the change in length that occurs upon deployment, to enable precise positioning during the implantation procedure [8]. Additionally, these devices should be self-expandable, meaning they should not undergo plastic deformations during the implantation procedure [10].

On one hand, various studies have proposed computational approaches to investigate the mechanical properties of bioresorbable braided stents [10–12], showing that the geometric characteristics of these devices significantly influence their mechanical performance. However, these studies have investigated a limited number of stent geometries and design parameters. On the other hand, geometry optimization approaches have been developed for laser-cut stents to extensively investigate the impact of the geometrical features on their mechanical performance, with the goal of identifying optimal device geometries and achieve superior treatment outcomes [13–25]. However, such geometry optimization approaches have been less frequently applied to braided stents [26–28], and they have not been utilized for bioresorbable braided stents. Therefore, the present study proposes a multi-objective geometry optimization framework based on the finite element (FE) modelling to optimize the mechanical performance of bioresorbable braided stents for the treatment of CLI.

2. Methods

The procedure applied for the optimization of bioresorbable braided stents involved the following main steps (Fig. 1): (i) development of a parametrized FE model of the stent to simulate the radial crimping test and assess the stent mechanical performance; (ii) formulation of the optimization problem by defining the optimization objectives, constraints and design space; (iii) integration of the design of experiments method with the surrogate modeling approach to establish an approximate relationship between the optimization objectives and constraints, and the design parameters of the stent; (iv) exploration of the design space to examine the impact of the design parameters on the stent mechanical performance; (v) multi-objective optimization to identify Pareto-optimal design candidates. Each step of the workflow is detailed in the following subsections.

2.1. Parametric FE model of the stent

A parametric FE model of a bioresorbable braided stent made of PLLA was developed. Its geometry was reconstructed using the approach proposed by Zaccaria et al. [29] and implemented in Matlab (MathWorks, Natick, MA, USA). This approach allows for the parametrization of the FE model by incorporating four design parameters associated with the stent geometry. These parameters include the number of wires of the stent (n), the diameter of the wire (d), the initial diameter of the stent (D_0), and the braiding angle of the stent (α) (Fig. 2). In detail, the braided stent geometry was obtained using parametric equations of a helix, in which a sinusoidal modulation of the radial component was added to describe the wire intertwining. The parametric equations for a single wire running in counterclockwise and clockwise directions, as indicated in Fig. 2, are represented by Eqs. (1) and 2, respectively:

$$\begin{cases} x(\theta) = \left(\frac{D_0+2d}{2} + \frac{d}{2}\cos\left(\theta\,\frac{n}{2} + \pi\right)\right)\cos(\theta) \\ y(\theta) = \left(\frac{D_0+2d}{2} + \frac{d}{2}\cos\left(\theta\,\frac{n}{2} + \pi\right)\right)\sin(\theta) \\ z(\theta) = \frac{D_0+2d}{2}\;\theta\,\tan(\alpha) \end{cases} \quad (1)$$

$$\text{with } \theta \in \left[0, \frac{2l_0}{(D_0+2d)\,\tan(\alpha)}\right]$$

$$\begin{cases} x(\theta) = \left(\frac{D_0+2d}{2} + \frac{d}{2}\cos\left(\theta\,\frac{n}{2}\right)\right)cos(-\theta) \\ y(\theta) = \left(\frac{D_0+2d}{2} + \frac{d}{2}\cos\left(\theta\,\frac{n}{2}\right)\right)sin(-\theta) \\ z(\theta) = \frac{D_0+2d}{2}\;\theta\,\tan(\alpha) \end{cases} \quad (2)$$

$$\text{with } \theta \in \left[0, \frac{2l_0}{(D_0+2d)\;tan(\alpha)}\right]$$

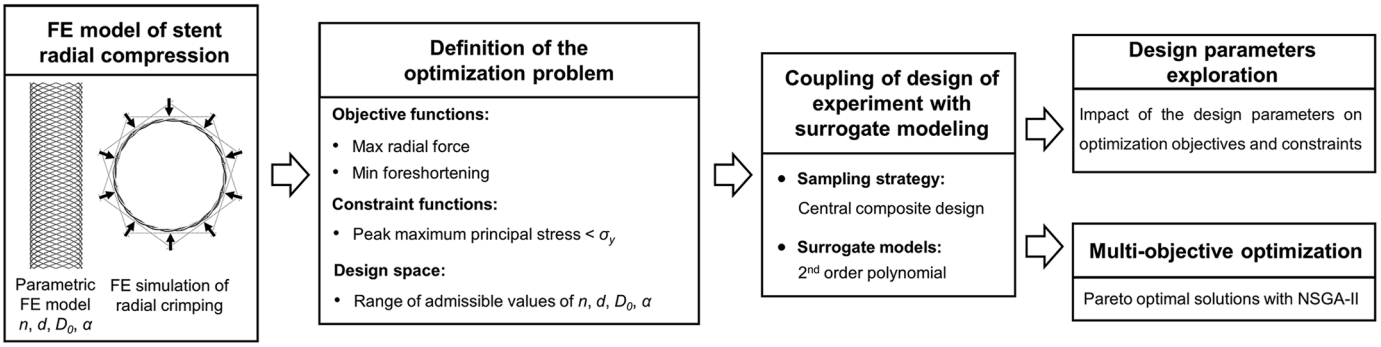

Fig. 1. Main steps of the optimization framework: (i) development of a parametrized FE model of the stent and FE simulation of the radial crimping test, taking into consideration four design parameters of the stent (see Sections 2.1, 2.2, 2.3 and 3.1); (ii) formulation of the optimization problem by defining the optimization objectives, constraints and design space (see Section 2.4.1); (iii) design parameters sampling and implementation of surrogate models of the optimization objectives and constraints (see Sections 2.4.2 and 3.2.1, and Supplementary material); (iv) exploration of the design space to investigate the impact of the design parameters on the optimization objectives and constraints (see Section 3.2.2); (v) multi-objective optimization to identify Pareto-optimal candidates of the stent designs (see Sections 2.4.3 and 3.3). n is the total number of wires of the stent, d is the diameter of the wire, D_0 is the initial diameter of the stent, α is the braiding angle of the stent."

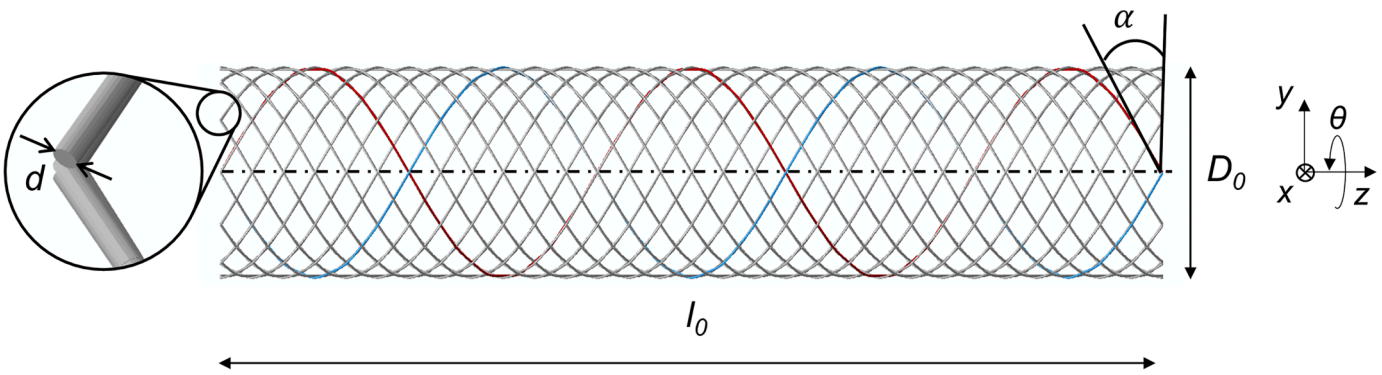

Fig. 2. Bioresorbable braided stent geometry. The red and blue wires of the stent correspond to the single counterclockwise and clockwise wires, respectively, as represented in Eqs. (1) and (2). The stent is formed by a total number of wires equal to *n*. *d* is the diameter of the wire, D_0 is the initial diameter of the stent, α is the braiding angle of the stent, l_0 is the initial length of the stent and θ is the polar angle that parametrize the geometry. *n, d,* D_0 and α are the four design parameters investigated in this study.

in which *n, d,* D_0 and α are the design parameters of the stent. The polar angle θ parametrizes the geometry and its maximum value is calculated based on the number of revolutions needed to achieve a an initial stent length (l_0) (Fig. 3) of 20 mm, chosen based on the study by Lucchetti et al. [30]. Finally, the counterclockwise and clockwise wires were cyclically repeated to generate the remaining structure, composed of a total of *n* wires. The stent geometry was then discretized in Matlab and exported as an input file for Abaqus/Explicit (Dassault Systèmes Simulia Corp., Johnston, RI, USA), which was considered as the reference FE solver. The stent geometry was discretized using B31 Timoshenko beam elements. The mesh density was determined based on a previous study [29]. The stent mechanical properties were obtained from a previous experimental study on bioresorbable braided stents [30]. Specifically, Fig. 3 illustrates the uniaxial stress-strain curve of PLLA obtained from tensile tests conducted on wire samples. An elasto-plastic constitutive law was employed to model the PLLA, incorporating the material model parameters reported in Table 1 and implementing the material plasticity curve based on the data shown in Fig. 3.

2.2. FE simulation of stent radial crimping

The radial crimping test is a standard method commonly used to characterize the mechanical performance of stents [31–33]. It aims to simulate the loading conditions that the stent during insertion into a catheter and deployment at the treatment site. FE analyses of the radial crimping were performed using Abaqus/Explicit on a single node of a cluster, equipped with 48 Cores (2 Intel Xeon Platinum 8160 processors

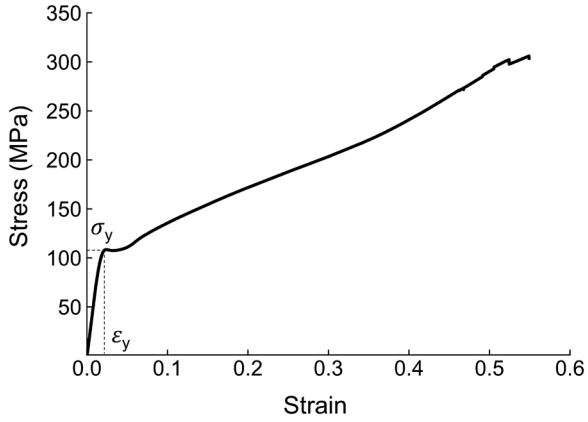

Fig. 3. Uniaxial stress *vs.* strain curve of PLLA obtained from tensile tests conducted on PLLA wires by Lucchetti et al. [30]. σ_y is the yield stress and ε_y is the yield strain. Their values are reported in Table 1.

Table 1
Mechanical properties of PLLA as measured by Lucchetti et al. [30], with reference to Fig. 3.

E	υ	σ_y	ε_y	ρ
6.4 GPa	0.35	110 MPa	0.03	1.25 g/cm^3

E: Young modulus, υ: Poisson ratio, σ_y: yield stress, ε_y yield strain, ρ density.

@2.10 GHz) and 192 GB RAM. The radial crimping of the stent was achieved through contact with ten rigid plates, which were radially translated (Fig. 4(a)), without any nodes of the stent being constrained. The rigid plates replicate the testing machine typically employed in experimental radial crimping tests [30,34]. The plates were modelled as rigid. Each plate was discretized using 90 R3D4 elements [35]. The radial crimping procedure consisted of two steps, namely the crimping and expansion steps (Fig. 4(a)). In the crimping step, the stent was crimped starting from its initial diameter D_0 to the minimum diameter $D_{min} = 2.3$ mm (corresponding to a catheter of 7 Fr). In the expansion step, the device was released back to its initial diameter D_0. Interactions between the parts were implemented with the general contact algorithm, considering the default "hard" normal contact behavior, with tangential behavior defined using a friction coefficient of $\mu = 0.12$ for the stent/plates interaction, and a coefficient of $\mu = 0.30$ when self-contact between the stent struts was considered. The friction coefficients were evaluated through a combined computational and experimental approach applied to the PLLA braided stents reported in [30]. Furthermore, it was ensured that ratio of the kinetic energy to the total internal strain energy was less than 5%, to perform a quasi-static analysis [29].

The following FE outputs were computed to evaluate the mechanical performance of the stent and subsequently incorporated into the formulation of the optimization problem (Section 2.3):

(i) Radial force (*RF*) applied by the stent when it expands. It is essential that the implanted stent applies a sufficiently high *RF* the vessel wall in order to provide support to the diseased artery and prevent tissue prolapse [8,31,32]. In detail, Fig. 4(b) illustrates a typical *RF vs. D* curve of a radial crimping test of a bioresorbable braided stent, as reported by Lucchetti et al. [30]. In this study, *RF* was measured at different diameters ranging from $D_- = 3.5$ mm to $D_+ = 4.1$ mm (Fig. 4(b)). These diameters were considered as representative of the dimensions of different vessels in which the device is implanted. For the purpose of the analysis, a nominal vessel diameter $D_N = 3.8$ mm was considered for the device implantation. Consequently, the *RF* values RF_-, RF_N and

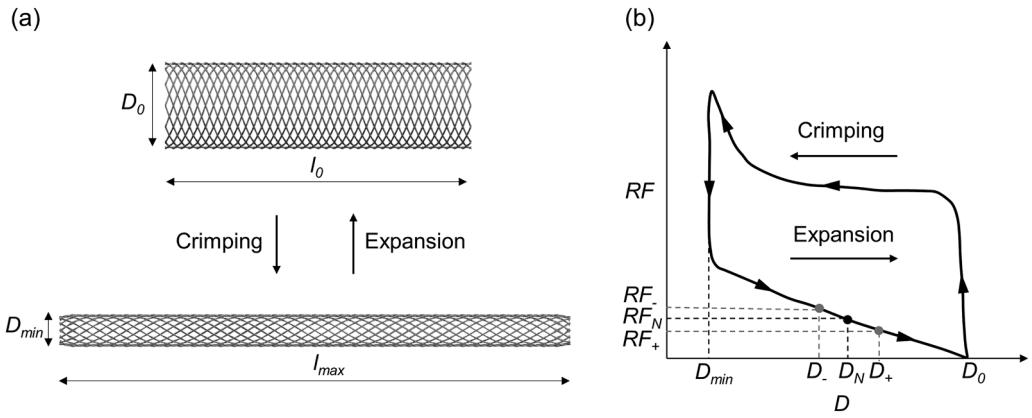

Fig. 4. (a) The radial crimping procedure, which comprises the crimping step followed by the expansion step. D_0, and D_{min} are the initial and minimum diameters, respectively. l_0 and l_{max}, are the initial and maximum lengths, respectively. (b) A typical *RF vs. D* curve for the radial crimping procedure of a bioresorbable braided stent. RF_-, RF_N and RF_+ are the *RF* values evaluated at the implantation diameters D_-, D_N and D_+ respectively, in the expansion step.

RF_+ were evaluated at the implantation diameters D_-, D_N and D_+, respectively (Fig. 4(b)). *RF* was computed for each *D* as the sum of the contact normal forces magnitudes measured on each plate, divided by l_0.

(ii) Foreshortening (*FS*) of the stent. Smaller *FS* values indicate higher precision in positioning the stent once it is expanded in the target location [8,31,32]. *FS* was evaluated at the minimum diameter (D_{min}), considering its maximum value throughout the radial crimping procedure. The *FS* was evaluated as $\frac{l_{max}-l_0}{l_0}$, where l_{max} is the length of the stent at D_{min} (Fig. 4(a)) [8].

(iii) Peak maximum principal stress (*PMPS*) within the stent. It is related to the structural integrity of bioresorbable braided stents [10]. To ensure a safe design, the upper limit value of *PMPS* was set equal to the yield stress σ_y of PLLA (Table 1), as depicted in the PLLA tensile loading curve of Fig. 3. The *PMPS* was measured at D_{min}, which conservatively represents the maximum value throughout the radial crimping procedure.

2.3. FE model validation

The results of the FE analysis of radial crimping were compared with the experimental test conducted in [30] on a braided stent made of the same material as the simulated device (Fig. 4). The stent used for comparison had the following characteristics: $n = 24$, $d = 0.1$, $D_0 = 5$ mm, $\alpha = 30°$, $l_0 = 20$ mm. Accordingly, an identical device was simulated, and the results were compared in terms of the outputs predicted by the FE simulation (i.e., RF_-, RF_N and RF_+).

2.4. Optimization procedure

2.4.1. Optimization objectives and constraints

The optimization of the biomechanical performance, as well as the associated clinical effectiveness, of the stent involved maximizing the *RF* generated during implantation, minimizing stent *FS*, and ensuring that the *PMPS* remained below σ_y. Specifically, the RF_N value was considered as a metric for the *RF* at implantation, which was targeted for maximization. Moreover, RF_- and RF_+ values were measured to evaluate the mechanical response within the range of implantation diameters.

The parameter design space of *n, d, D_0* and α was defined while considering the constraints imposed by manufacturing technology used for braided stents [36]. In particular, *n* was treated as a discrete variable, with possible values of 24, 32, 36, and 48, in accordance with the technical specifications of wire braiding machines. *d* was treated as a discrete variable with possible values of 0.05 mm, 0.075 mm, and 0.10 mm, based on availability from the PLLA wire supplier [30]. D_0 was assumed to vary continuously within the range of [4.5 mm, 5.5 mm], as it depends on the diameter of the braiding mandrel used in manufacturing, which can be custom-made to the desired diameter. Taking into account the range of implantation diameters [D_-, D_+], the oversizing ratios (i.e., D_0 divided by implantation diameter) were found to be within the range of $\left[\frac{D_0=4.5\ mm}{D_+=4.1\ mm} = 1.1,\ \frac{D_0=5.5\ mm}{D_-=3.5\ mm} = 1.6\right]$, which is consistent with previous investigations [37]. Lastly, α was treated as a continuous variable since braiding machines allow for continuous selection of this parameter, spanning the range of [20°, 30°], in accordance with previous experimental investigations [30].

Summarizing, the present optimization problem can be formulated as:

$$\begin{cases} \max\limits_{x \in DS} RF_N(\boldsymbol{x}) \\ \min\limits_{x \in DS} FS(\boldsymbol{x}) \\ s.t.: \begin{cases} PMPS(\boldsymbol{x}) < \sigma_y \\ DS = \begin{cases} \boldsymbol{x} = [n, d, D, \alpha]: \\ n \in \{24,\ 32,\ 36, 48\} \\ d \in \{0.05\text{ mm},\ 0.075\text{ mm},\ 0.10\text{ mm}\} \\ D_0 \in [4.5\text{ mm}, 5.5\text{ mm}] \\ \alpha\ \in [20°, 30°] \end{cases} \end{cases} \end{cases} \tag{3}$$

where $RF_N(\boldsymbol{x})$ and $FS(\boldsymbol{x})$ are the optimization objectives, $PMPS(\boldsymbol{x}) < \sigma_y$ is the non-linear constraint function, $\boldsymbol{x}$ is the vector of the design parameters and *DS* is the design space.

2.4.2. Surrogate modelling

Surrogate models were established for RF_-, RF_N, RF_+, *FS* and *PMPS*. The central composite design (CCD) (circumscribed) sampling strategy [38] was implemented in Hyperstudy (Altair Engineering, Troy, MI, USA), performing 25 sampling FE simulations of the radial crimping procedure. The number of samples was defined by the following equation [38]:

$$2^k + 2k + n_0 \tag{4}$$

where $k = 4$ is the number of design parameters and $n_0 = 1$ is the number of center points. The optimization objectives and constraint were calculated through the FE simulations, and the resulting data was exported in Matlab. Polynomial 2nd order surrogate models were implemented in Matlab to establish an approximate relationship between the design parameters and the optimization objectives and

constraint. Details on the validation of the surrogate models are provided in the Supplementary material.

2.4.3. Multi-objective optimization

The validated surrogate models were used to conduct a multi-objective optimization and identify sets of Pareto-optimal design candidates. The non-dominated sorting genetic algorithm (NSGA-II) [39] was employed in Matlab for this purpose. The settings of the algorithm are reported elsewhere [40–42]. A non-linear constraint function was also incorporated to ensure that the solutions obtained during the optimization process are feasible and adhere to the upper limit of the *PMPS* (see Eq. (3)). Finally, the identified Pareto-optimal solutions underwent a filtering process to eliminate duplicate solutions and prevent overlapping designs.

3. Results

3.1. FE model validation

Fig. 5 presents a comparison between experimental and FE simulation results of radial crimping for a selected PLLA braided stent. It includes the experimental radial crimping *RF vs. D* curve from Lucchetti et al. [30], along with the computed values of RF_-, RF_N, and RF_+ obtained through both experimental and FE analysis. The results demonstrate a good agreement between the experimental and FE analysis, with a maximum relative error of 11.6 % (Table 2).

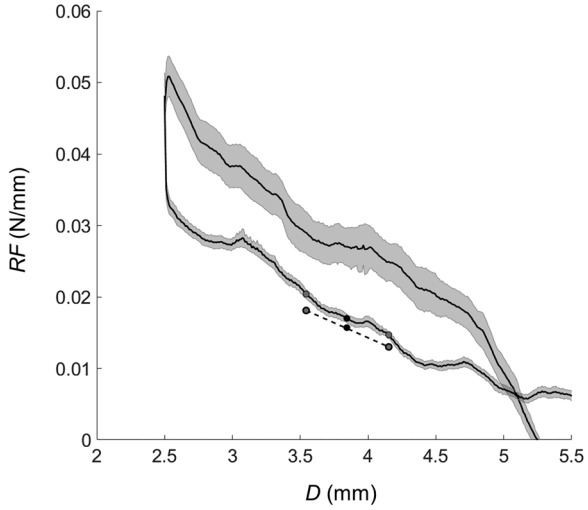

Fig. 5. Comparison of experimental and FE simulation results of radial crimping of a PLLA braided stent with the following characteristics: $n = 24$, $d = 0.1$ mm, $D_0 = 5$ mm, $\alpha = 30°$, $l_0 = 20$ mm. The black line and the shaded area represent the mean values and the standard deviations of the *RF vs. D* data, respectively, obtained from the experimental radial crimping test conducted by Lucchetti et al. [30]. Values of RF_-, RF_+, and of RF_N are represented by grey points and black points, respectively. The points lying on the black line represent experimental data, while the remaining points, connected by the dotted line, correspond to the results obtained from FE simulation.

Table 2
Comparison between experimental and FE simulation results of the RF_-, RF_N and RF_+ values.

	RF_-	RF_N	RF_+
Experimental	0.020 N/mm	0.017 N/mm	0.015 N/mm
FE simulation	0.018 N/mm	0.016 N/mm	0.013 N/mm
Relative error	11.3%	7.6%	11.6%

3.2. Surrogate modelling

3.2.1. Sampling FE simulations

Fig. 6 presents the objectives and constraint functions obtained from the 25 FE simulation samples of the CCD scheme. Fig. 6(a) shows the nominal value RF_N along with the values of RF_- and RF_+ for each FE simulation sample. It is evident that the nominal value RF_N is located approximately halfway between RF_- and RF_+, highlighting the linearity of the *RF vs. D* curve during the expansion step at implantation (see Fig. 5). Furthermore, the magnitude of $|RF_- - RF_+|$ rises as the RF_N values increase, indicating an enhanced slope of the *RF vs. D* curve. Fig. 6(b) displays the *FS* values, with reported values up 1.75. Fig. 6(c) depicts the *PMPS* values, which were found to be lower than σ_y. It is observable that higher values of RF_N correspond to higher values of *PMPS*. The broad range of values observed for both objective functions RF_N and *FS* suggests the potential to achieve favorable outcomes in terms of optimized quantities. Further details can be found in the Supplementary material (Tables S2 and S3).

Fig. 7 shows the axial displacement and maximum principal stress contour plot for the FE simulation sample 1, represented in red in Fig. 6. The contour plot reveals that the stent undergoes axial elongation in both positive and negative directions. Additionally, the maximum principal stress is evenly distributed along the stent length, with peak values concentrated at the contact zones between the stent struts.

3.2.2. Design parameters exploration

The surrogate models were successfully validated. The results of the validation process are reported in the Supplementary material (Fig. S1 and Table S1).

The validated surrogate models were utilized to examine the influence of each design parameter on the optimization objectives and constraint. The curves of RF_N (together with RF_- and RF_+), *PMPS* and *FS* obtained by varying one parameter at time while maintaining the others fixed at the median value (see Eq. (3)), are depicted in Fig. 8. Fig. 8(a) shows that RF_N is primarily affected by n, d, and α, with d having the highest impact. Increasing n and d enhances the device radial stiffness, leading to higher radial forces during radial compression. Furthermore, decreasing α increases the radial component of the generated contact forces. Conversely, the initial stent diameter D_0 appears to have a marginal impact on the RF_N. Furthermore, RF_- and RF_+ exhibit a similar trend to RF_N, with slight increasing values of $|RF_+ - RF_-|$ as RF_N increases. Fig. 8(b) shows that *FS* is markedly impacted only by α. This can be attributed to the fact that *FS* depends on the motion of the stent during radial compression, which is primarily affected by α. Finally, Fig. 8(c) demonstrates that *PMPS* is mainly impacted by d and α, with d having the greatest influence. Moreover, the contrast between RF_N and *PMPS* was observed for d and α, but not for n. Increasing n leads to the force being distributed over a greater number of wires, which accounts for this distinction.

3.3. Multi-objective optimization

Fig. 9(a) depicts the sets of non-dominated optimal solutions lying on the Pareto-front of the two objective functions, RF_N and *FS*, which characterize the mechanical performance of PLLA braided stents. A comparable trend is observable among RF_N, RF_- and RF_+, with similar values of $|RF_- - RF_+|$ for all optimal design candidates. Thirteen Pareto-optimal design candidates were identified from the multi-objective optimization, and their characteristics are listed in Table 3. It can be observed that all optimal design candidates have $n = 48$, $d = 0.10$ mm and D_0 values that slightly vary but tend towards 4.5 mm. Additionally, the optimal designs exhibit α values in the the range of $[20°, 30°]$. Fig. 9 (b) presents the *PMPS* values of the optimal design candidates, indicating that all of the optimal design candidates have feasible *PMPS* values.

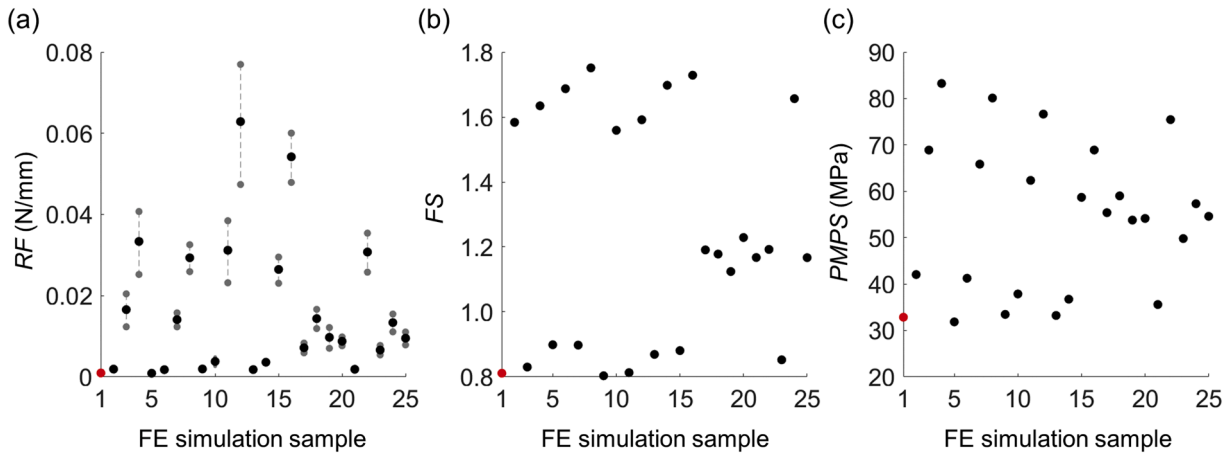

Fig. 6. Objectives and constraint values as obtained from the 25 FE simulation samples of the CCD scheme. (a) RF_N values are represented as black points, while the RF_- and RF_+ values are depicted as grey points connected by a dotted line, where the highest and lowest points correspond to RF_- and RF_+, respectively; (b) *FS* values; (c) *PMPS* values. The red point refers to the FE simulation sample 1.

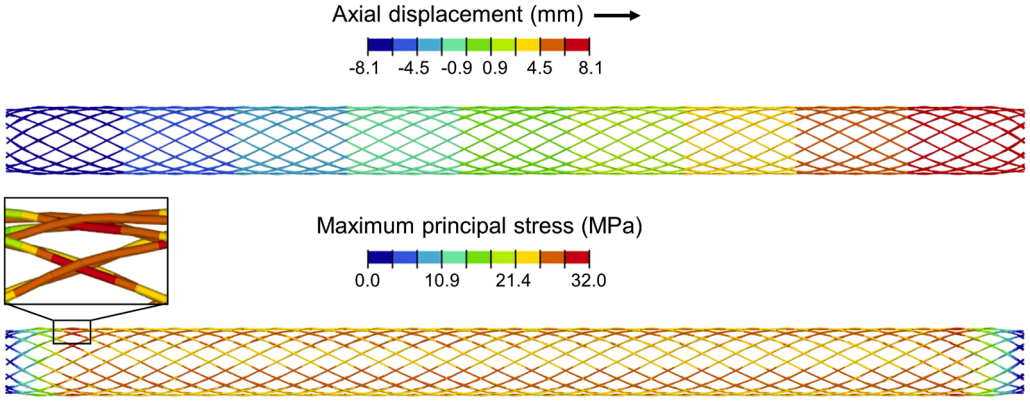

Fig. 7. Contour plot of the axial displacement and maximum principal stress of the FE simulation sample 1, indicated in red in Fig. 6. FE simulation sample 1 is characterized by $n = 24$, $d = 0.05$ mm, $D_0 = 4.5$ mm and $\alpha = 30°$. The arrow in the upper legend represents the axial direction.

4. Discussion

The use of computational modeling tools offers valuable assistance in the design and development phases of vascular stents [43]. By reducing the reliance on multiple prototypes and experimental tests, these tools positively impact product development cycle time and costs. Furthermore, computer modeling and simulation enable the optimization of stent designs, facilitating the systematic creation of devices with improved mechanical performance and potentially superior clinical outcomes, thereby overcoming the limitations of the trial-and-error approach. Bioresorbable braided stents are innovative devices that have been underexplored computationally [10]. This study presents, for the first time, an optimization framework specifically designed for such a type of stents, with the goal to enhance their mechanical characteristics, thus potentially overcoming existing limitations and enhancing their clinical effectiveness in the treatment of CLI.

The optimization framework incorporated the replication of the radial crimping test, following the specified standard [31,32], through FE analysis to characterize the mechanical performance of bioresorbable braided stents. The FE analysis of radial crimping was compared to a corresponding experimental test conducted on a selected stent design. The comparison revealed a good agreement between the numerical and experimental results in terms of *RF* evaluated at the implantation diameters.

All the FE models samples generated through CCD simulations resulted in correct geometries and were successfully simulated, showcasing the potential of the parametric FE model of the bioresorbable braided stent in conducting the design of experiments. The computational cost of the optimization procedure was primarily influenced by the FE simulations, whereas the automatic generation of FE models and the multi-objective optimization incurred negligible computational expenses (< 5 min). Specifically, each FE simulation necessitated up to 10 h on our cluster, resulting in a CCD sampling phase totaling approximately 250 hours in the worst-case scenario where FE simulation samples could not be parallelized. Surrogate models were successfully implemented and validated, establishing an approximate relationship between RF_-, RF_N, RF_+, *FS* and *PMPS* and the four design parameters. In this regard, an initial investigation was carried out by varying one design parameter at a time while keeping the others fixed at the median value (Fig. 8). This approach provided valuable insights into the impact of design parameters on the predicted objectives and constraint functions and may facilitate decision-making in stent design based on predicted mechanical behavior. However, this approach involved a limited exploration of the design space. Therefore, a multi-objective optimization procedure was subsequently performed, leading to the identification of optimal design candidates with enhanced mechanical characteristics within the design space. Interestingly, the Pareto-optimal design candidates exhibited feasible PMPS values, indicating that the optimization process successfully satisfied the constraint (Fig. 9(b)). These candidates were characterized by upper bounds of $n = 48$ and $d = 0.01$ mm, as increasing these parameters resulted in higher RF_N values without compromising *FS* (Fig. 8). Additionally, the

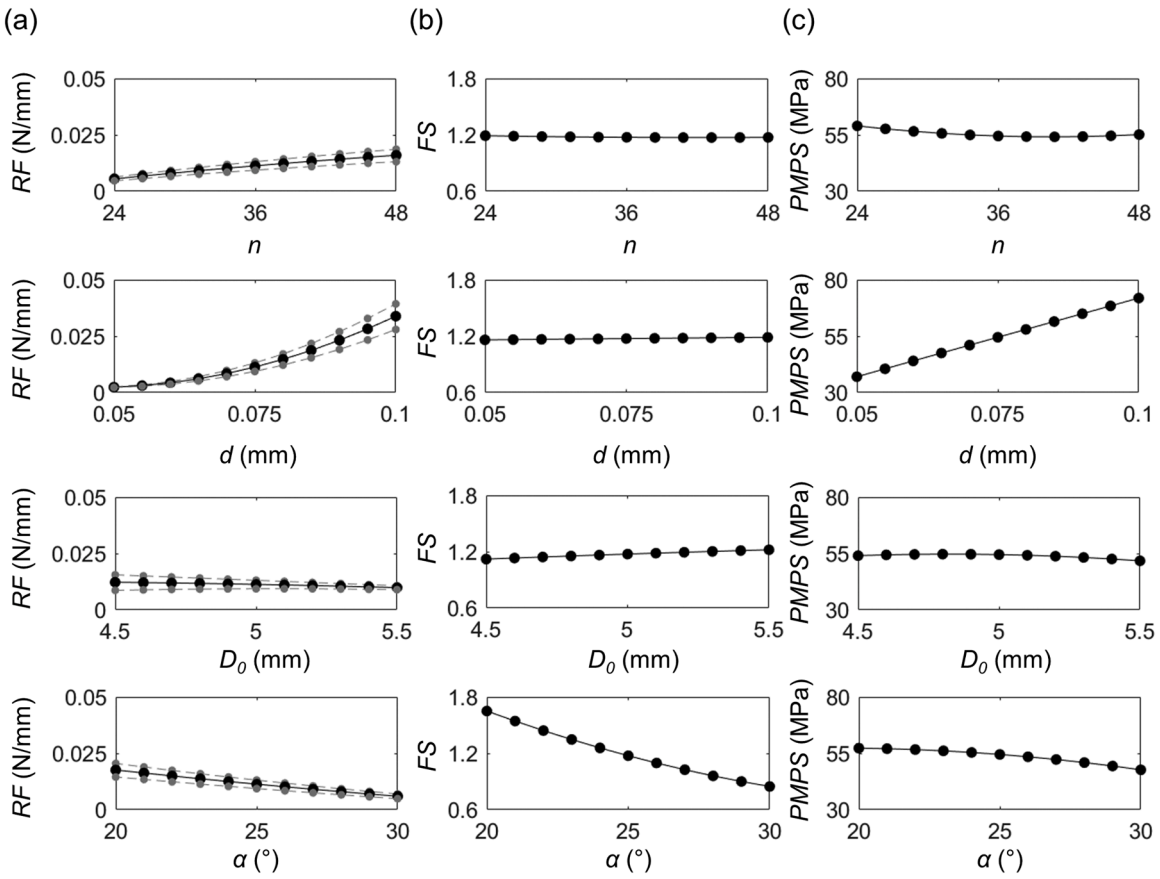

Fig. 8. Predicted values of (a) RF_-, RF_N, RF_+, (b) *FS* and (c) *PMPS* by the surrogate models by varying one parameter at time while maintaining the others fixed at the median value. Median values of the design parameters (see Eq. (1)) are $n = 36$, $d = 0.075$ mm, $D_0 = 5$ mm and $\alpha = 25°$. (a) The black line refers to RF_N, and the upper and lower grey lines refer to RF_- and RF_+, respectively.

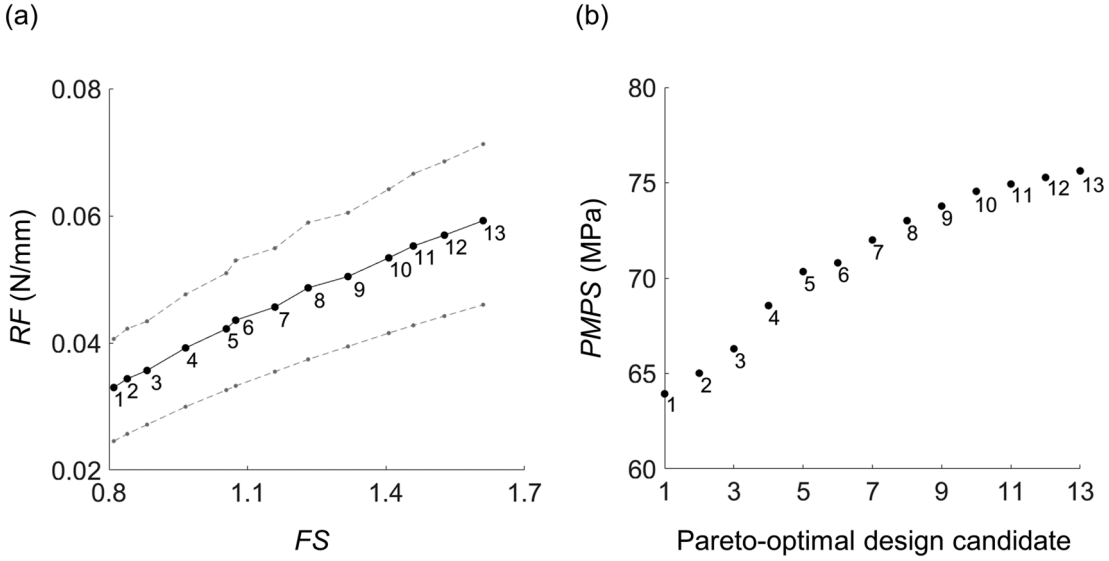

Fig. 9. (a) Pareto-front of RF_N *vs. FS*, depicted as a black line, where each point corresponds to a Pareto-optimal design candidate. The corresponding RF_- and RF_+ values are illustrated as grey dotted lines. (b) *PMPS* values of the identified Pareto-optimal design candidates.

candidates had D_0 values close to the lower bound of 4.5 mm, as decreasing D_0 slightly increased RF_N while maintaining *FS* (Fig. 8). Consequently, the key differentiating factor among the candidates was found to be the parameter α (Table 3).

This study presents some limitations. The optimization procedure did not consider the feasible values of *RF* and *FS* that bioresorbable braided stents should meet for CLI applications, as relevant literature data on this aspect were unavailable. Additional studies should be conducted to investigate the radial force that stents need to generate for CLI applications, considering variations in the characteristics of the

Table 3
Design parameters of the Pareto optimal design candidates, represented in Fig. 9.

Optimal design candidate	n	d (mm)	D_0 (mm)	α (°)
1	48	0.10	4.51	30.0
2	48	0.10	4.52	29.4
3	48	0.10	4.59	28.8
4	48	0.10	4.59	27.4
5	48	0.10	4.62	26.2
6	48	0.10	4.55	25.8
7	48	0.10	4.65	24.8
8	48	0.10	4.57	23.9
9	48	0.10	4.66	23.0
10	48	0.10	4.62	22.1
11	48	0.10	4.58	21.5
12	48	0.10	4.60	20.8
13	48	0.10	4.60	20.0

n: number of wires of the stent; d: the diameter of the wire; D_0: initial diameter of the stent; α: braiding angle of the stent.

specific diseased vessel. Furthermore, the optimization focused solely on simulating the radial crimping of the device, which effectively measures *RF, FS*, and *PMPS* during the implantation procedure. However, *in vivo* conditions involve more complex loading conditions [44] that could be considered through additional mechanical tests to fully characterize the device behavior. Moreover, to address the potential risk of thrombosis associated with bioresorbable stents [1], further advancements could be implemented to optimize the hemodynamics of the devices. Finally, the optimization framework was applied to solely one PLLA braided stent design, considering a restricted extension of the design space, based on the constraints imposed by manufacturing technology [36] and on a previous experimental study [30]. Nevertheless, the framework provided enough flexibility to be extended to different bioresorbable materials, braided stent designs and, in general, braided cardiovascular devices.

5. Conclusions

The computational framework proposed in this study proved to be effective in assessing the influence of geometric characteristics on the mechanical performance of bioresorbable braided stents. It successfully identified optimal design candidates that exhibited enhanced mechanical characteristics, considering realistic manufacturing constraints. This contribution aids in the advancement of innovative bioresorbable braided stents for the effective treatment CLI, while also reducing time and costs associated with the iterative development and prototyping phases of the device.

Funding

DC, ALA and CC were supported by the Piedmont Region, Italy [POR FESR PiTeF 2014-20 351-96, Nitiliera]. TJV and AL were supported through a project that has received funding from the European Union's Horizon 2020 research and innovation programme under grant agreement No 813869. This publication reflects only the author's view and the REA is not responsible for any use that may be made of the information it contains.

CRediT authorship contribution statement

Dario Carbonaro: Conceptualization, Methodology, Software, Investigation, Data curation, Validation, Writing – original draft, Writing – review & editing. **Agnese Lucchetti:** Methodology, Software, Investigation, Data curation, Validation, Writing – original draft, Writing – review & editing. **Alberto L. Audenino:** Writing – review & editing, Funding acquisition. **Thomas Gries:** Writing – review & editing, Funding acquisition. **Ted J. Vaughan:** Methodology, Writing – review & editing, Supervision. **Claudio Chiastra:** Methodology, Writing – original draft, Writing – review & editing, Supervision.

Declaration of Competing Interest

The authors declare that they have no conflict of interest.

Acknowledgements

None.

Supplementary materials

Supplementary material associated with this article can be found, in the online version, at doi:10.1016/j.cmpb.2023.107781.

References

[1] X. Wu, S. Wu, H. Kawashima, H. Hara, M. Ono, C. Gao, R. Wang, M. Lunardi, F. Sharif, W. Wijns, P.W. Serruys, Y. Onuma, Current perspectives on bioresorbable scaffolds in coronary intervention and other fields, Expert Rev. Med. Devices. 18 (2021), https://doi.org/10.1080/17434440.2021.1904894.
[2] H.Y. Ang, J. Ng, H. Bulluck, P. Wong, S. Venkatraman, Y. Huang, N. Foin, Fundamentals of bioresorbable stents, Funct. Cardiovasc. Stents (2017), https://doi.org/10.1016/B978-0-08-100496-8.00005-6.
[3] B. Forrestal, B.C. Case, C. Yerasi, A. Musallam, C. Chezar-Azerrad, R. Waksman, Bioresorbable scaffolds: current technology and future perspectives, Rambam Maimonides Med. J. 11 (2020), https://doi.org/10.5041/RMMJ.10402.
[4] H. Jinnouchi, S. Torii, A. Sakamoto, F.D. Kolodgie, R. Virmani, A.V. Finn, Fully bioresorbable vascular scaffolds: lessons learned and future directions, Nat. Rev. Cardiol. 16 (2019), https://doi.org/10.1038/s41569-018-0124-7.
[5] K. Nakka, S.D. Nagarajan, B. Sundaravadivel, S. Shankaravel, C. Vimalson, An overview of the design, development and applications of biodegradable stents, Drug Deliv. Lett. 10 (2019), https://doi.org/10.2174/2210303109666190617165344.
[6] N. Katib, R.L. Varcoe, The state of stenting in below-the-knee applications, Endovasc. Today 20 (2021).
[7] M. Henry, C. Klonaris, M. Amor, I. Henry, K. Tzvetanov, State of the art: which stent for which lesion in peripheral interventions? Texas Hear. Inst. J. 27 (2000).
[8] C. Pan, Y. Han, J. Lu, Structural design of vascular stents: a review, Micromachines 12 (2021), https://doi.org/10.3390/mi12070770.
[9] N. Korei, A. Solouk, M. Haghbin Nazarpak, A. Nouri, A review on design characteristics and fabrication methods of metallic cardiovascular stents, Mater. Today Commun. 31 (2022), https://doi.org/10.1016/j.mtcomm.2022.103467.
[10] J. Li, J. Cheng, X. Hu, J. Liu, Y. Tian, G. Wu, L. Chen, Y. Zhang, G. Zhao, Z. Ni, A hazardous boundary of Poly(L-lactic acid) braided stent design: limited elastic deformability of polymer materials, J. Mech. Behav. Biomed. Mater. 138 (2023), https://doi.org/10.1016/j.jmbbm.2022.105628.
[11] F. Zhao, W. Xue, F. Wang, J. Sun, J. Lin, L. Liu, K. Sun, L. Wang, Braided bioresorbable cardiovascular stents mechanically reinforced by axial runners, J. Mech. Behav. Biomed. Mater. 89 (2019), https://doi.org/10.1016/j.jmbbm.2018.09.003.
[12] C. Shanahan, S.A.M. Tofail, P. Tiernan, Viscoelastic braided stent: finite element modelling and validation of crimping behaviour, Mater. Des. 121 (2017), https://doi.org/10.1016/j.matdes.2017.02.044.
[13] H. Wang, L. Jiao, J. Sun, P. Yan, X. Wang, T. Qiu, Multi-objective optimization of bioresorbable magnesium alloy stent by kriging surrogate model, Cardiovasc. Eng. Technol. 13 (2022), https://doi.org/10.1007/s13239-022-00619-1.
[14] Ł.A. Mazurkiewicz, J. Bukała, J. Małachowski, M. Tomaszewski, P.P. Buszman, BVS stent optimisation based on a parametric model with a multistage validation process, Mater. Des. 198 (2021), https://doi.org/10.1016/j.matdes.2020.109363.
[15] R. Gharleghi, H. Wright, V. Luvio, N. Jepson, Z. Luo, A. Senthurnathan, B. Babaei, B.G. Prusty, T. Ray, S. Beier, A multi-objective optimization of stent geometries, J. Biomech. 125 (2021), https://doi.org/10.1016/j.jbiomech.2021.110575.
[16] N.W. Bressloff, G. Ragkousis, N. Curzen, Design optimisation of coronary artery stent systems, Ann. Biomed. Eng. 44 (2016), https://doi.org/10.1007/s10439-015-1373-9.
[17] D. Carbonaro, F. Mezzadri, N. Ferro, G. De Nisco, A. Luigi, D. Gallo, C. Chiastra, U. Morbiducci, S. Perotto, Design of innovative self-expandable femoral stents using inverse homogenization topology optimization, Comput. Methods Appl. Mech. Eng. 416 (2023), 116288, https://doi.org/10.1016/j.cma.2023.116288.
[18] G. Alaimo, F. Auricchio, M. Conti, M. Zingales, Multi-objective optimization of nitinol stent design, Med. Eng. Phys. 47 (2017), https://doi.org/10.1016/j.medengphy.2017.06.026.
[19] N.S. Ribeiro, J. Folgado, H.C. Rodrigues, Surrogate-based multi-objective design optimization of a coronary stent: altering geometry toward improved biomechanical performance, Int. J. Numer. Method. Biomed. Eng. 37 (2021), https://doi.org/10.1002/cnm.3453.
[20] S. Pant, N.W. Bressloff, G. Limbert, Geometry parameterization and multidisciplinary constrained optimization of coronary stents, Biomech. Model. Mechanobiol. 11 (2012), https://doi.org/10.1007/s10237-011-0293-3.

[21] S. Pant, G. Limbert, N.P. Curzen, N.W. Bressloff, Multiobjective design optimisation of coronary stents, Biomaterials 32 (2011), https://doi.org/10.1016/j.biomaterials.2011.07.059.
[22] W. Wu, L. Petrini, D. Gastaldi, T. Villa, M. Vedani, E. Lesma, B. Previtali, F. Migliavacca, Finite element shape optimization for biodegradable magnesium alloy stents, Ann. Biomed. Eng. 38 (2010), https://doi.org/10.1007/s10439-010-0057-8.
[23] R. Clune, D. Kelliher, J.C. Robinson, J.S. Campbell, NURBS modeling and structural shape optimization of cardiovascular stents, Struct. Multidiscip. Optim. 50 (2014), https://doi.org/10.1007/s00158-013-1038-y.
[24] S. Tammareddi, G. Sun, Q. Li, Multiobjective robust optimization of coronary stents, Mater. Des. 90 (2016), https://doi.org/10.1016/j.matdes.2015.10.153.
[25] N. Li, H. Zhang, H. Ouyang, Shape optimization of coronary artery stent based on a parametric model, Finite Elem. Anal. Des. 45 (2009), https://doi.org/10.1016/j.finel.2009.01.001.
[26] M. De Beule, S. Van Cauter, P. Mortier, D. Van Loo, R. Van Impe, P. Verdonck, B. Verhegghe, Virtual optimization of self-expandable braided wire stents, Med. Eng. Phys. 31 (2009), https://doi.org/10.1016/j.medengphy.2008.11.008.
[27] H. Yu, L. Zheng, J. Qiu, J. Wang, Y. Xu, B. Fan, R. Li, J. Liu, C. Wang, Y. Fan, Mechanical property analysis and design parameter optimization of a novel nitinol nasal stent based on numerical simulation, Front. Bioeng. Biotechnol. 10 (2022), https://doi.org/10.3389/fbioe.2022.1064605.
[28] R. Ubachs, O. Van Der Sluis, S. Smith, J. Mertens, Journal of the mechanical behavior of biomedical materials computational modeling of braided venous stents — effect of design features and device-tissue interaction on stent performance, J. Mech. Behav. Biomed. Mater. 142 (2023), https://doi.org/10.1016/j.jmbbm.2023.105857.
[29] A. Zaccaria, F. Migliavacca, D. Contassot, F. Heim, N. Chakfe, G. Pennati, L. Petrini, Finite element simulations of the ID venous system to treat venous compression disorders: From model validation to realistic implant prediction, Ann. Biomed. Eng. 49 (2021), https://doi.org/10.1007/s10439-020-02694-8.
[30] A. Lucchetti, C. Emonts, A. Idrissi, T. Gries, T.J. Vaughan, An experimental investigation of the mechanical performance of PLLA wire-braided stents, J. Mech. Behav. Biomed. Mater. 138 (2023), https://doi.org/10.1016/j.jmbbm.2022.105568.
[31] FDA, Non-clinical engineering tests and recommended labeling for intravascular stents and associated delivery systems, (2010).
[32] ISO, Cardiovascular implants — Endovascular devices — Part 2: Vascular stents, (2012).
[33] C.G. McKenna, T.J. Vaughan, An experimental evaluation of the mechanics of bare and polymer-covered self-expanding wire braided stents, J. Mech. Behav. Biomed. Mater. 103 (2020), 103549, https://doi.org/10.1016/j.jmbbm.2019.103549.
[34] T. Matsumoto, Y. Matsubara, Y. Aoyagi, D. Matsuda, J. Okadome, K. Morisaki, K. Inoue, S. Tanaka, T. Ohkusa, Y. Maehara, Radial force measurement of endovascular stents: Influence of stent design and diameter, Vascular 24 (2016), https://doi.org/10.1177/1708538115590040.
[35] L. Antonini, L. Mandelli, F. Berti, G. Pennati, L. Petrini, Validation of the computational model of a coronary stent: a fundamental step towards in silico trials, J. Mech. Behav. Biomed. Mater. 122 (2021), https://doi.org/10.1016/j.jmbbm.2021.104644.
[36] Y. Kyosev, Braiding technology for textiles: Principles, design and processes, 2014.
[37] C. Gökgöl, N. Diehm, F.R. Nezami, P. Büchler, Nitinol stent oversizing in patients undergoing popliteal artery revascularization: a finite element study, Ann. Biomed. Eng. 43 (2015), https://doi.org/10.1007/s10439-015-1358-8.
[38] N.R. Draper, D.K.J. Lin, Response surface designs, 1996.
[39] K. Deb, A. Pratap, S. Agarwal, T. Meyarivan, A fast and elitist multiobjective genetic algorithm: NSGA-II, IEEE Trans. Evol. Comput. 6 (2002), https://doi.org/10.1109/4235.996017.
[40] D. Carbonaro, D. Gallo, U. Morbiducci, A. Audenino, C. Chiastra, In silico biomechanical design of the metal frame of transcatheter aortic valves: multi-objective shape and cross-sectional size optimization, Struct. Multidiscip. Optim. 64 (2021), https://doi.org/10.1007/s00158-021-02944-w.
[41] D. Carbonaro, S. Zambon, A. Corti, D. Gallo, U. Morbiducci, L. Audenino, C. Chiastra, Impact of nickel – titanium super-elastic material properties on the mechanical performance of self-expandable transcatheter aortic valves, J. Mech. Behav. Biomed. Mater. 138 (2023), https://doi.org/10.1016/j.jmbbm.2022.105623.
[42] A. Corti, M. Colombo, J.M. Rozowsky, S. Casarin, Y. He, D. Carbonaro, F. Migliavacca, J.F.R. Matas, S.A. Berceli, C. Chiastra, A predictive multiscale model of in-stent restenosis in femoral arteries: linking haemodynamics and gene expression with an agent-based model of cellular dynamics, J. R. Soc. Interface 19 (2022), https://doi.org/10.1098/rsif.2021.0871.
[43] T.M. Morrison, M.L. Dreher, S. Nagaraja, L.M. Angelone, W. Kainz, The role of computational modeling and simulation in the total product life cycle of peripheral vascular devices, J. Med. Devices, Trans. ASME. 11 (2017), https://doi.org/10.1115/1.4035866.
[44] L. Haghighat, S.E. Altin, R.R. Attaran, C. Mena-Hurtado, C.J. Regan, Review of the latest percutaneous devices in critical limb Ischemia, J. Clin. Med. 7 (2018), https://doi.org/10.3390/jcm7040082.